# Journal of Materials Chemistry B

Accepted Manuscript




This is an *Accepted Manuscript*, which has been through the Royal Society of Chemistry peer review process and has been accepted for publication.

*Accepted Manuscripts* are published online shortly after acceptance, before technical editing, formatting and proof reading. Using this free service, authors can make their results available to the community, in citable form, before we publish the edited article. We will replace this *Accepted Manuscript* with the edited and formatted *Advance Article* as soon as it is available.

You can find more information about *Accepted Manuscripts* in the Information for Authors.

Please note that technical editing may introduce minor changes to the text and/or graphics, which may alter content. The journal's standard Terms & Conditions and the Ethical guidelines still apply. In no event shall the Royal Society of Chemistry be held responsible for any errors or omissions in this *Accepted Manuscript* or any consequences arising from the use of any information it contains.



ROYAL SOCIETY OF CHEMISTRY

www.rsc.org/materialsB

# Low-Cost Photo-Responsive Nanocarrier Platform by One-Step Functionalization of Flame-made Titania Agglomerates with L-lysine

Tina Zhang[1], Mary A. Go[2], Christian Stricker[2], Vincent R. Daria[2] and Antonio Tricoli[1]*

[1]Nanotechnology Research laboratory, Research School of Engineering, Australian National University, Canberra, Australia

[2]John Curtin School of Medical Research, Australian National University, Canberra, Australia

*Tel.: +61 (0)2 612 51696. Email: antonio.tricoli@anu.edu.au

Keywords: Stimuli-Responsive, Flame Synthesis, Drug Delivery, Neuron, Two-Photon Microscope, Amino Acids.

**Abstract**

A novel versatile photo-responsive nanocarrier able to load and release several functional molecules is obtained by one-step conjugation of scalable flame-made Titania agglomerates. Highly crystalline anatase nano-crystals are synthesized by scalable flame spray pyrolysis of organometallic precursor solutions. Nanocarriers are self-assembled by adsorption of a lysine molecule on the photocatalytic nanoparticle surface leading to minimal flocculation and highly reactive amine terminations. Time-controlled photo-release of the ligand and end-loaded molecules is achieved by short UV light exposure. Application of these flexible nanoplatforms to intracellular delivery is demonstrated by dye loading and two-photon microscopy in-vitro imaging of their penetration in living neurons of Wistar rat brain tissue. These scalable photo-responsive nanocarriers are a flexible platform with potential for *in-vivo* controlled release of amine-reactive dyes and amino-acid modified pro-drugs as demonstrated by successful loading and release of fluorescein isothiocyanate dye (FITC) and ketoprofen.

## 1. Introduction

In the last decade, targeted drug-delivery has attained significant achievements by leveraging on the synthesis of novel stimuli-responsive nanocomposites made of multi-functional organic-inorganic structures[1]. For example, key anti-cancer drugs, such as paclitaxel and docetaxel, used to be difficult to deliver due to their hydrophobic nature[2], are now supplied with the aid of substrates such as noble metals[3], metal oxides[4], polymers[5], and solid lipids[6]. The sub-cellular size of nanocomposites facilitates penetration into tissues facilitating internalization[7] and, recently, enabling direct intracellular photo-stimulation[8] . The release of drugs and other functional molecules may occur passively by diffusion, as a response to changes in pH[9] , progressive degradation of the substrate material[10], temperature change[11], or actively such as by magnetic and ultrasonic resonance[12] and photocleavage[13]. The last is attractive as it offers superior release control and can be externally triggered in the body by pulsed electromagnetic radiations such as UV light[14]. Such light-responsive nanocarriers can now deliver doxorubicin[15, 16], sulforhodamine 101[17] and chlorambucil[18].

Titania is one of the most efficient photocatalysts and is a promising photo-responsive carrier material. Electron/hole separation in $TiO_2$ can be triggered by electromagnetic radiation having energies above the material band gap such as ultraviolet light[19] and X-rays[20]. $TiO_2$ can be made on the commercial scale using flame spray deposition, a cost-effective and highly scalable process. Flame-made $TiO_2$ nanoparticles are usually agglomerated with a fractal-like, elongated morphology[21]. Optimization of the flame synthesis conditions enables control of the particle collision frequency leading to more[22] or less[23] agglomerated nanostructures and tunable primary particle size. The nanocomposite size and morphology has a major impact on the final drug delivery efficiency. For example, small particles (≈ 20 - 30 nm) have demonstrated higher uptake in cancer tissues[24] by endocytosis but suffer from high reticuloendothelial (RES) clearance. In contrast, particles of ca. 100 - 200 nm have shown among the best overall performance as they are sufficiently large to avoid renal filtration and vascular fenestration (cut-off of ca. 5 and 50 nm, respectively), and sufficiently small to attach to the tumor endothelium[25]. Additionally, non-spherical particles and elongated structures can improve circulation time, and thus delivery efficiency, by decreasing

Journal of Materials Chemistry B Accepted Manuscript

phagocytosis rate[26]. In this respect, the use of hard-agglomerated $TiO_2$ nanoparticles as photo-responsive substrates presents several advantages.

Flame-made $TiO_2$ surfaces are usually amphoteric and can therefore load functional molecules through acid-base chemistry as well as adsorption through charge attractions. The five-fold coordinate Ti atoms act as Lewis acids, and O atoms serving as base. Hydroxylation of their surface results in aqueous medium results in Brønsted acid and base such as terminal Ti-OH and rooted O-H[27] enabling adsorption of organic acids[28], bases[29], silanes[30] and phosphonates[31]. However, direct loading of most drugs on the $TiO_2$ surface by robust chemisorption is challenging due to the poor reactivity of hydroxyl groups. Enhancement of the loading capability of $TiO_2$ agglomerates by conjugating amino acids to act as flexible ligands is attractive. It can enable the loading of several bioactive molecules. Among others, lysine is a key amino acid in proteins that has shown potential for several applications such as vaccine delivery[32], DNA carrier[33], and stem-cell labelling[34].

Reaction with anti-inflammatory drug ketoprofen to form lysine-ketoprofen prodrug is particularly attractive. Ketoprofen being ordinarily hydrophilic cannot easily cross the blood-brain-barrier (BBB) unless modified by amino acids to allow for transport across the large amino acid transporters, and thereafter biodegradation of the lysine-ketoprofen link to yield pharmacologically active ketoprofen.[35] Optimization of lysine binding[36] is essential for obtaining high and specific reactivity toward the target drug, sufficiently small particle sizes and rapid resulting release under UV stimulation. In fact, lysine features several binding configurations on the $TiO_2$ surface by either its amine or carboxylic groups,[27, 28] and has so far led to the formation of polypeptide layers on $TiO_2$ surfaces with drastically reduced loading capacity. Instead, ketoprofen reacts with lysine via amide formation between the lysine's ε-$NH_2$ and the –COOH of ketoprofen, and thus require active amine terminations.[37]

Here, we present the scalable fabrication of a photo-responsive nanocarrier platform by rapid flame-synthesis and one-step conjugation of ultra-fine $TiO_2$ agglomerates with lysine. Highly crystalline anatase nanoparticles with controlled primary particle and agglomerate sizes are produced in by flame spray pyrolysis of organometallic precursor solutions. Lysine conjugation is investigated over a broad spectrum of reaction pH, time and concentrations resulting in efficient nanocarriers with high loading capacity, minimal flocculation and encapsulation. The ligand release dynamics and efficiency is investigated by time-controlled UV-exposure. The performance of this flexible nanoplatform is demonstrated by loading and release of ketoprofen and fluorescein isothiocyanate dye (FITC). Their suitability for intracellular delivery is assessed by two-photon microscope imaging of their three-dimensional distributions in living neurons as a function of their key structural properties.

## 2. Experimental

### 2.1 Flame Synthesis of $TiO_2$ Agglomerates

A flame spray pyrolysis (FSP) reactor was used for the synthesis of $TiO_2$ nanoparticles (Supporting Materials, Figure S1) as previously discussed in detail[22]. The liquid precursor was prepared by diluting 0.5 mol $^{-1}$ of titanium (IV) isopropoxide (TTIP, Aldrich, purity > 97%) in xylene (Fluka, purity > 98.5%). The solution was supplied at a rate of 5 ml $min^{-1}$ through the FSP nozzle and dispersed to a fine spray with 5 l $min^{-1}$ oxygen (pressure drop 6 bar) through the surrounding annulus. That spray was ignited by a supporting annular ring of premixed methane/oxygen flamelets ($CH_4$ = 1.2 l $min^{-1}$, $O_2$ = 2 l $min^{-1}$). Powder samples were collected with a vacuum pump (ICME Type M80B4) on water-cooled glass fibre filters (Sartorius glass microfiber FT-3-01124-150, 160 mm diameter) placed at ca. 40 cm height above the burner (HAB). X-ray diffraction analysis was performed with a Bruker, D2 Phaser diffractometer operated at 30 kV, 10 mA at 2θ (Cu Kα) = 10° - 80°, step = 0.02° and scan speed = 2.3° $min^{-1}$. The crystal size ($d_{XRD}$) was determined by Rietveld analysis with the structural parameters of rutile and anatase. The powder specific surface area (SSA) was measured by BET analysis using a Micromeritics Tristar II. The BET equivalent diameter was calculated for spherical primary particles using the XRD weighted average densities of $TiO_2$ rutile and anatase. Transmission electron microscopy was conducted in a Hitachi H2100, operated at 125 kV.

Journal of Materials Chemistry B Accepted Manuscript

### 2.2 Ligand Conjugation and Characterization

Conjugation was carried out in aqueous solutions at pH 9, pH 7 and pH 1.5 prepared by adding HCl (Aldrich, purity > 37%), and NaOH (Aldrich, purity > 97%) to distilled water. The pH was measured using a pH probe (Oakton pH 700) at the start of reaction. The $TiO_2$ powders were first calcined in a muffle furnace (CEMMS) for 4 h at 450 °C to desorb physi- or chemisorbed $H_2O$. Thereafter, 9 ml of 5.23 mmol $l^{-1}$ $TiO_2$ nanoparticle suspensions were prepared by adding 3.76 mg of $TiO_2$ powder to the aqueous solutions and ultrasonicating (Eumax Ultrasonic Cleaner) for 5 min. A controlled amount of L-lysine (Aldrich, purity > 98%) was dissolved in the aqueous solutions and added to the particle suspensions. The L-lysine concentration was dosed with respect to the amount required (1 monolayer, ML) for complete conjugation of the $TiO_2$ surface metal atoms. The monolayer lysine concentration was estimated as following: a maximal theoretical Ti-metal atom surface concentration of 12.43 atom $nm^{-2}$ was computed resulting from the XRD composition and considering only the most thermodynamically stable surface planes of anatase (101) and rutile (110), and a spherical geometry of single diameter ($d_{BET}$). All surface Ti atoms were assumed to be in this active hydroxylated configuration for stoichiometry calculations. In line with previous studies[27, 28], five possible binding configurations of L-lysine (Supporting Materials, Figure S2) to these Ti-OH binding sites were considered: (a) physisorption through (the more reactive) ε-amine, and carboxylate binding via (b) hydrogen bonding, (c) ester binding, (d) chelating and (e) bridging states. Cases (a) to (d) lead 1:1 ratio between -OH groups and lysine molecules, while (e) results in a 2:1 ratio. Based on the 1:1 configuration, excess, stoichiometric and sub-stoichiometric amounts of L-lysine were added to each solution. First, 10 mg, 1.46 mg and 0.75 mg of L-lysine in were dissolved into 1 ml of aqueous solution at the desired pH. This was then added to the nanoparticle suspensions. The reaction proceeded at room temperature, with magnetic stirring at 600 rpm and the effect of reaction time was investigated from 0 to 500 h. The functionalized nanoparticles were collected from the reaction medium via centrifugation at 4000 rpm for 40 min. The particles were washed once in water and re-suspended in distilled water solutions. A Zetasizer Nano S (Malvern) was used to measure change in zeta (ζ)-potential and hydrodynamic diameter ($d_H$) between as-prepared and lysine-conjugated nanoparticles. Transmission electron microscope (TEM) (Hitachi 2100, operated at 125kV) was used to determine the formation of a polylysine matrix. ATR-FTIR (Bruker Alpha) was used to determine the resulting bonding type.

### 2.3 Functional Molecule Loading and Release

The prepared $TiO_2$ particle-lysine solutions were ultrasonicated in a bath sonicator (Eumax UD100SH-3LN, 100 W) for additional 3 min to break-up potential soft agglomerates. Thereafter, 10 ml of 1 mmol $l^{-1}$ fluorescein isothiocyanate I (Sigma, purity > 90%) diluted in a water/ethanol solution (e.g. 1:9 volume ratio) was added in to the $TiO_2$ particle-lysine solutions to create dye-labelled nanostructures. To form ketoprofen-lysine-$TiO_2$ structures, 10mL aliquots of lysine-$TiO_2$ were first centrifuged at 4000 rpm for 50 minutes to remove supernatant, then freeze-dried for 2hrs. Ketoprofen (5mg) (Sigma, purity > 98%), and 4-(Dimethylamino)pyridine (0.3mg) (Sigma, purity > 99%) were dissolved in dry dichloromethane (30mL) (Sigma, purity > 99.8%) and ethanol (20mL) (Sigma, > 99.8%) before adding to dried lysine-$TiO_2$ particles, followed by 10 minutes ultrasonication to form suspension before addition of N-cyclohexy-N'-(2-morpholinoethyl)carbodiimide-metho-p-toluenesulphonate (4.6mg) (Sigma, >99%). Both FITC and ketoprofren loading was performed at room temperature for 48h with stirring at 300 rpm, after which the samples were centrifuged again at 4000 rpm for 50 min to separate product. The collected FITC and ketoprofen-terminated nanocomposites were suspended in water solutions by ultrasonication for an additional 3 min. These solutions were analyzed by ζ-potential (Malvern Zetasizer Nano S) and UV-vis absorption measurements (Tecan M200Pro) to quantify the degree of loading and surface composition. To photocleave the ligand, the suspended product was exposed to UV light of 365 nm, 100 W (Spectroline Model SB700P/FA). Eluent was separated by centrifugation at 4000 rpm for 50 minutes. The effect of exposure time was investigated by dynamic light scattering and ζ-potential for each sample (Malvern Zetasizer Nano S). Primary amine fluorescamine assays were performed on eluent by

Journal of Materials Chemistry B Accepted Manuscript

adding 100µL of 1 mg $mL^{-1}$ fluorescamine in DMSO to 300uL of sample solution with fluorescence emission recorded at 470 nm (Tecan M200Pro). GC-MS was used to identify released lysine and ketoprofen. Samples were injected (0.2 – 1.0 µl injection volume) via an autosampler onto a Rtx-5MS fused-silica capillary column (Restek, Bellefonte, PA, USA; 30m x 0.25mm id) coated with a 5% phenyl-95% dimethylpolysiloxane (0.25µm film thickness) which was eluted with He (inlet pressure 14.5 psi) directly into the ion source of a Thermo Polaris Q GC/MS (injection port 220°C; interface 250°C; source 250°C). The column was temperature programmed from 80 °C (hold 1 min) to 300 °C at 10°C $min^{-1}$. The mass spectrometer was operated in the electron impact ionisation (EI) mode with ionisation energy of 70 eV and scanned from m/z 50 to m/z 400.

### 2.4 Neuron Preparation and Imaging

Using a vibratome (Leica VT 1200S), parasagittal brain slices (300 µm thick) of Wistar rat brain (P15-22) were prepared. The slices were cut in ice-cold oxygenated artificial cerebrospinal fluid (ACSF) containing 1.25 mmol $l^{-1}$ $NaH_2PO_4$, 1.0 mmol $l^{-1}$ $MgCl_2$, 125.0 mmol $l^{-1}$ NaCl, 2.5 mmol $l^{-1}$ KCl, 2.0 mmol $l^{-1}$ $CaCl_2$, 25.0 mmol $l^{-1}$ $NaHCO_3$ and 10.0 mmol $l^{-1}$ glucose. Slices were incubated in oxygenated ACSF at 34 °C for 30 min and kept at room temperature before transferal to the recording chamber. Functionalized nanoparticle suspensions containing 418 mg $l^{-1}$ $TiO_2$ were added to an intracellular solution containing 115 mmol $l^{-1}$ K-gluconate, 20 mmol $l^{-1}$ KCl, 10 mmol $l^{-1}$ HEPES, 10 mmol $l^{-1}$ phosphokreatine, 4 mmol $l^{-1}$ ATP-Mg, 0.3 mmol $l^{-1}$ GTP and 5.4 mmol $l^{-1}$ biocytin and patch pipettes (R = 4-5 MΩ) back-filled with this solute. Neurons in the somatosensory cortex or hippocampus were recorded from using the whole-cell recording technique with a Multi Clamp 700B. This solution was then allowed to diffuse into layer II/III pyramidal neurons through the recording pipette 20-30 min before imaging. Current was injected when necessary to maintain a resting membrane potential of -70 mV. Neurons were imaged at 800 nm with 12-22 mW laser power. Image stacks of 800×800 pixels in a single plane were generated by imaging individual planes in 1 µm increments along the z-axis. ImageJ (National Institute of Health) was used for 3D visualization. Experiments on animal tissue were performed under a protocol approved by the Animal Ethics Committee of the Australian National University.

## 3. Results and Discussion

### 3.1 Flame Synthesis of Nanostructured $TiO_2$ Agglomerates

Highly crystalline $TiO_2$ nanoparticle agglomerates were synthesized in one step by flame spray pyrolysis of titanium tetraisopropoxide combustible solutions (Figure 1a). The particle size distribution and composition were optimized by controlling oxygen dispersion, precursor feed rate and concentration as previously reported[23]. High precursor concentration (0.5 mol $l^{-1}$) and feed-rate (5 ml $min^{-1}$) were used to ensure scalability of the nanocarrier synthesis process and structural properties[38]. The XRD analysis (Supporting Materials, Figure S3) of the collected powders revealed a highly crystalline material without any detectable amount of amorphous phase and impurity. Rietveld analysis of the XRD spectra indicated a small content of rutile (13%) and a predominant anatase phase (87%) with average crystal sizes of 20.9 nm. This was in agreement with the BET analysis indicating a specific surface area (SSA) of 73 $m^2$ $g^{-1}$ and a primary particle size of ($d_{BET}$) 21 nm. The $TiO_2$ band-gap estimated by UV-vis light absorption was ca. 3.35 eV, and thus comparable to that previously reported for flame-made $TiO_2$[39]. The powder isoelectric point and the zeta potential in neutral conditions (deionized water solutions) were pH 3.5 and -40 mV (Table 1), respectively.

Journal of Materials Chemistry B Accepted Manuscript

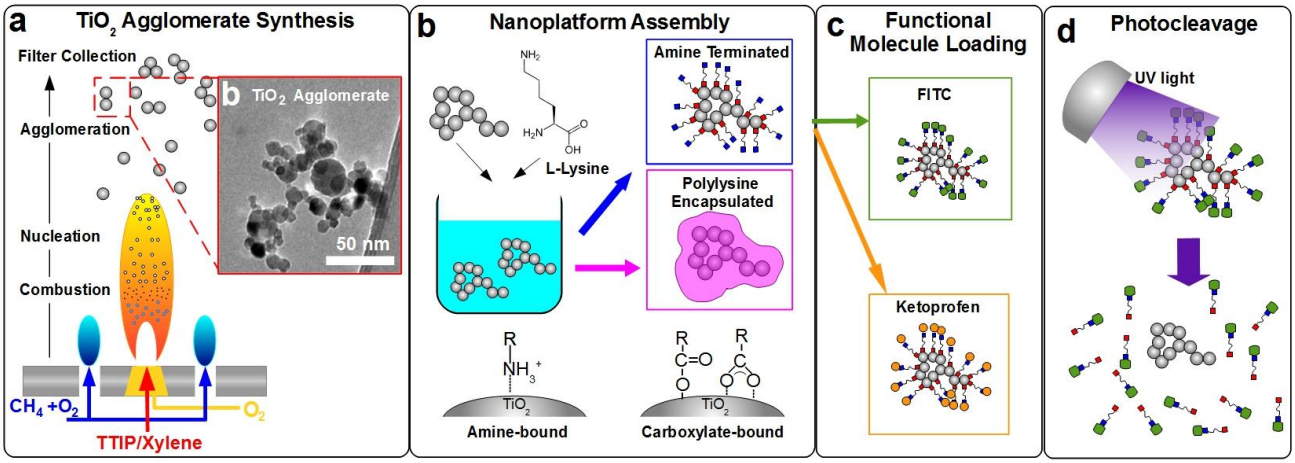


**Figure 1.** *Nanocarrier assembly schematic by (a) flame pyrolysis synthesis of $TiO_2$ nanoparticle agglomerates and (b) functionalization with L-lysine in pH-controlled aqueous solutions. The flexibility and broad applicability of these optimal nanocarriers was assessed by loading of (c) a FITC dye and ketoprofen. Photo-induced release (d) was demonstrated by short exposure (≤ 30 s) to UV light.*

TEM analysis of the as-prepared powders (Figure 2a) revealed an agglomerated morphology displaying elongated, fractal-like chain of $TiO_2$ nanoparticles up to 200 nm in length. At higher magnification (Figure 2b), the agglomerates were identified as clusters of $TiO_2$ primary particles with size between 5 and 50 nm. This is in good agreement with the measured $d_{BET}$ and $d_{XRD}$ diameters of 21 and 20.9 nm, respectively, and with previous reports on flame-made $TiO_2$ powders[22, 40] produced at similar conditions. Here, dynamic light scattering analysis showed a unimodal particle size distribution with a hydrodynamic diameter ($d_H$) of 180 nm and a quasi-lognormal shape ($\sigma_g$ =1.306). This distribution corresponds to the fractal structure of hard agglomerates formed by the sintering of primary particles in the flame[38] and its fraction and shape were found to be consistent across different batches. This is in good agreement with the agglomerate size distribution reported for flame-made $SnO_2$ nanoparticles[38, 41]. This degree of agglomeration is attributed to the Brownian coagulation and sintering of the primary particles during the high temperature residence time in the flame[38]. Most importantly, the $TiO_2$ agglomerate size obtained here is sufficiently large (> 50 nm) to maximize circulation time for drug delivery avoiding both renal filtration and vascular fenestration while their elongated chain-like morphology (Figure 2a) is expected to inhibit phagocytosis[26].

**Table 1.** Zeta potential and mean hydrodynamic diameter ($d_H$) before and after 68h lysine conjugation at 7 ML.

| **Material** | **ζ (mV)** | **$d_H$(nm)** |
|---|---|---|
| As-prepared $TiO_2$ | -40.0 | 180 |
| Lysine Conjugated $TiO_2$ at pH 9 | +1.09 | 3000 |
| Lysine Conjugated $TiO_2$ at pH 1.5 | +13.0 | 700 |

ζ = Zeta potential, $d_H$ = Hydrodynamic diameter

### 3.1 Ligand Attachment and Nanocarrier Assembly

To enable loading of functional molecules, these flame-made agglomerates were conjugated with lysine (Figure 1b), aiming to obtain highly reactive amine surface terminations. Conjugation was initially investigated as a function of reaction pH and time for over-stoichiometric lysine concentrations corresponding theoretically to seven-monolayer coverage. Upon conjugation for 68 h, the mean ζ-potential (Table 1) increased from -40 mV for the as-prepared $TiO_2$ to +1.09 mV and +13.0 mV for alkaline and acidic conditions, respectively. This suggests that in alkaline conditions (ζ-potential = +1.09 mV) physisorption through the lysine amine groups (Figure 1) is the dominant mechanism. This is in good agreement with the theoretical zero ζ-potential expected for lysine physisorption (Supporting Materials, Figure S2). In contrast, the positive surface charging (+13.0 mV), measured in acidic conditions, is attributed to lysine chemisorption by its carboxylic ending. These may form (Figure 1) either carboxylic hydrogen bonds (ester-like monodentate and chelating forms) or carboxylic

Journal of Materials Chemistry B Accepted Manuscript

bridging with a theoretical ζ-potential of +80 mV and +40mV, respectively. The carboxylic biding achieved here is attributed to the solution being adequately acidic to deprotonate the surface of Ti-OH, but not sufficiently to fully protonate the dissociated -$COO^-$ [36]. As a result acidic conjugation was necessary to terminate the $TiO_2$ surface with active amine groups.

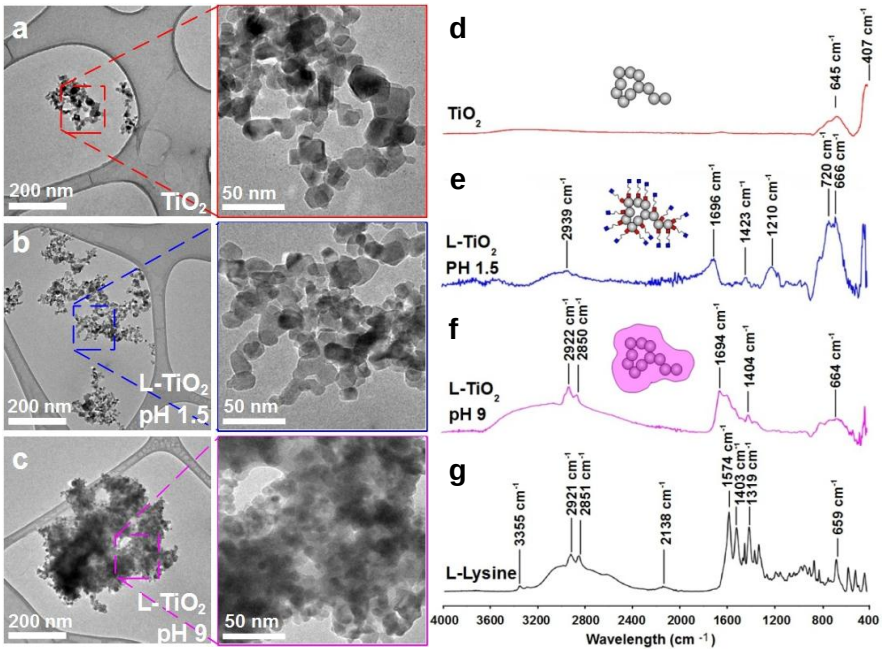


**Figure 2.** TEM images of the as-prepared (a), and lysine-functionalized (7 ML concentration, $t_r$ = 68h) $TiO_2$ nanoparticles at pH 9 (b) and 1.5 (c). FTIR absorbance spectra of as-prepared $TiO_2$ (d), nanoparticles functionalized with lysine (7 ML concentration, $t_r$ = 68h) at pH 1.5 (e) and pH 9 (f), and pure solid L-lysine (g).

The reaction pH was also the key process parameter controlling the final agglomerate size. In alkaline conditions, the hydrodynamic diameter ($d_H$) increased by ca. 15 folds from 180 nm of the as-prepared flame-made agglomerates to 3000 nm of the lysine-$TiO_2$ nanocarriers (Table 1). This is in line with the neutral ζ-potential measured for alkaline conjugation leading to minor electrostatic repulsion, and thus strong flocculation. This was further confirmed by their TEM analysis (Figure 2c) showing very large spherically-shaped structures. This encapsulated morphology (Figure 1b) differs from the as-prepared $TiO_2$ showing a majority of elongated chain-like structures (Figure 2a). This is attributed to the high flocculation in alkaline conditions leading to rotation symmetric growth. At higher magnification, a thick amorphous matrix encapsulating several $TiO_2$, agglomerates was observed. This suggests that in alkaline conditions polylysine is formed. This is in agreement with pH dependence of $TiO_2$ surface charge and dominant form of L-lysine. At pH 9, $TiO_2$ surfaces possess negative charge (Supplementary Materials Figure S7), while L-lysine is zwitterionic, allowing for simultaneous attraction between protonated -$NH_3^{3+}$ and particle surface and lysine-lysine interactions in the form of amide formation or hydrogen bonding[42] between -$COO^-$ and -$NH_3^{3+}$. As a result, here, the significant increase in agglomerate size to 3000 nm for alkaline conjugation is attributed to the increased flocculation rate arising from the neutral surface charging, and the higher sticking likelihood of the amine-functionalized $TiO_2$ surface.

In contrast, acidic conjugation (7ML for 68 h) led to relatively small variations from the initial $TiO_2$ agglomerate size and morphology. The hydraulic diameter of these nanocarriers was 700 nm (Table 1), showing a 3 to 4 folds increase from the as-prepared powders. This is attributed to the relatively long reaction time (68 h) leading to some (limited) flocculation also in alkaline conditions. However, the nanocarrier morphology (Figure 2b) was hardly distinguishable from that of the pure $TiO_2$ agglomerates (Figure 2a) showing fractal-like elongated nanostructures. At higher magnification, the $TiO_2$ particle surface was clearly visible with no indications of the amorphous matrix observed for alkaline conjugation (Figure 2d). This suggests

Journal of Materials Chemistry B Accepted Manuscript

successful functionalization of $TiO_2$ with a thin lysine layer (Figure 1b) and is a considerable improvement over encapsulation with polylysine (Figure 1b)[43, 44].

Figure 2 shows the FTIR spectra of (d) as-prepared, (e) acidic and (f) alkaline conjugated $TiO_2$ (L-$TiO_2$), and a solid L-lysine sample (g). The as-prepared $TiO_2$ (Figure 2d) spectrum was characterized by strong absorption bands below 850 $cm^{-1}$. These are attributed to the lattice vibrations of $TiO_2$[41], and confirm the high crystallinity of the flame-made samples. The spectrum of the acidic conjugated samples (Figure 2e) was similar to that of the as-prepared $TiO_2$ showing few peaks matching the lysine spectrum (Figure 2g). This further supports the successful formation of a lysine monolayer as indicated by the TEM analysis (Figure 2b). A unique feature of the acidic samples was the presence of a 1210 $cm^{-1}$ peak not identifiable in the pure $TiO_2$ (Figure 2d) and alkaline (Figure 2f) ones. This is attributed to the overlap of two vibrational modes belonging to the C-O stretch of the ester formed between the $TiO_2$ surface -OH groups and the amine terminations of lysine. This indicates the formation of covalent bonds between lysine and $TiO_2$.

Conjugation in alkaline conditions (Figure 2f) resulted in significantly higher match to the polylysine spectrum (Figure 2g) with a similar broad hump between 3600-2000 $cm^{-1}$. This is characteristic of solid polylysine (PLL) samples dried upon polypeptide reactions in highly alkaline conditions (pH ~12)[45] and it is commonly attributed to the overlapping bands of $NH^+$ groups[46]. Here, this $NH^+$ surge is attributed to the formation of disordered, dendritic polypeptide layers terminating in protonated amino groups. Another distinguishing feature of the alkaline samples is an intense peak at 1645 $cm^{-1}$ corresponding to the C=O vibration of amide structures formed during peptide assembly. The sharp peaks at 2922 $cm^{-1}$ and 2850 $cm^{-1}$ (Figure 2f) are assigned to $CH_2$ bonds[45]. Their intensity increases rapidly with polypeptide chain formation. These results confirm further that, in alkaline conditions, polylysine is prevalently formed while acidic conjugation leads to covalent carboxylic bonding enabling $TiO_2$ functionalization with a lysine monolayer.

To further optimize the final nanocarrier size and surface properties, the acidic conjugation dynamics was investigated for stoichiometric (1 ML) and sub-stoichiometric (0.5 ML) lysine concentrations. The ζ-potential time-evolution indicated a different chemical kinetics for the 0.5 ML (Supporting Materials, Figure S4, empty circles) and 1 ML (Supporting Materials, Figure S4, full circles) samples. While at 1 ML typical diffusion-limited profiles were obtained, the 0.5 ML solutions had a delayed chemical response with a nearly constant ζ-potential up to ca. 60h. However, both concentrations reached a maximum ζ-potential after 200-300 h reaction time before converging toward +20 mV. This maximum may arise from the formation of a monolayer of bonded lysine. The subsequent decrease is attributed to the flocculation of the nanocarriers resulting in the increased hydrodynamic diameter (700 nm) and agglomerate size (Figure 2b) observed for the 7 ML acidic conjugation.

This conjugation dynamics was supported by the size distribution dynamics measured by dynamic light scattering (DLS). Upon 2.5h reaction, both the 0.5 and 1 ML samples evolved from a unimodal (Figure 3a,b, black lines) into a tri-modal size distribution (Figure 3a,b, blue lines). The latter was characterized by a low intensity peak (ca. 80-100 nm) partially overlapping with the initial unimodal peak, a main peak at ca. 600 nm, and a final peak at 5000-6000 nm. The first peak was attributed to non-flocculated particles representing the agglomerates of the initial distribution. The second and third peaks were attributed to the formation of secondary agglomerates through the binding of multiple as-prepared $TiO_2$ agglomerates. Increasing the lysine concentration from 0.5 ML (Figure 3a) to 1 ML (Figure 3b) increased the relative intensity of this third peak indicating an acceleration of the flocculation rate. Similarly, increasing the lysine reaction time (> 2.5h) rapidly increased the relatively intensity of the third peak (Figure 3a,b blue line) while decreasing the first two modes. At 1 ML lysine concentration, a reaction time of 250h (Figure 3b, dark blue line) resulted in the formation of a quasi-unimodal distribution with a hydrodynamic diameter of ca. 6000 nm. These results indicate that even in acidic conditions, the surface charges formed on the $TiO_2$ agglomerates are not sufficient to fully stabilize the original agglomerate size and thus lysine conjugation time must be

Journal of Materials Chemistry B Accepted Manuscript

limited to avoid extensive agglomeration. Here, optimal nanocomposite morphologies with high concentration of surface amine groups and limited agglomerate size were found to form in acidic environments and short (≤ 2.5h) reaction times.

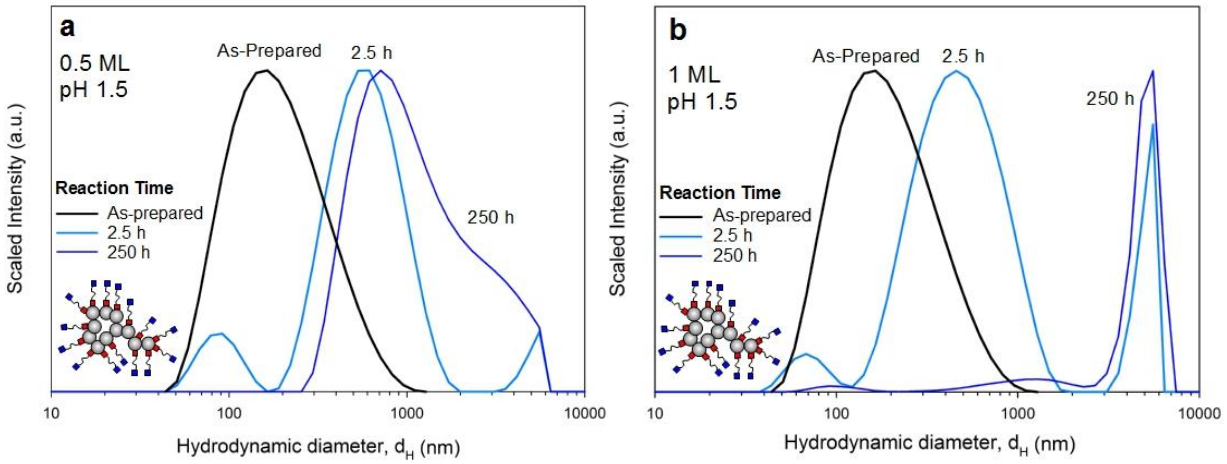


**Figure 3.** *Hydrodynamic diameter ($d_H$) size distribution measured by dynamic light scattering as a function of reaction time at pH 1.5, for (a) 0.5 ML and (b) 1 ML lysine concentrations.*

### 3.2 Functional Molecule Loading and Photo-Induced Time-Controlled Release

The loading capacity and flexibility of these photo-responsive nanoplatforms was quantified by terminating the lysine ligand with and a fluorescent dye (FITC), commonly utilized for cell imaging, and ketoprofen, an anti-inflammatory drug whose cell membrane permeability may be drastically enhanced when modified with lysine[37]. With respect to the former, for all samples, the UV-absorption spectra of the FITC-terminated composites (Figure 7a,b, green lines) confirmed the presence of a peak at ca. 492 nm. This corresponds to the excitation wavelength of the FITC dye and was not present in the as-prepared (red line) and lysine conjugated sample (magenta line). FITC-$TiO_2$ without adsorbed lysine (Figure 7a, black line) was used a control and proved that direct adsorption of FITC onto $TiO_2$ was negligible. For all lysine concentrations, the FITC peak increased with decreasing conjugation pH from alkaline (Figure 7a,b dark green line) to acidic (Figure 7a,b light green line) conditions. Decreasing the lysine conjugation concentration from 7 ML (Figure 7a) to 1 ML (Figure 7b) led to a drastic increase in adsorbed dye. This indicates that, independently of the reaction pH, lower lysine concentration leads to higher available surface and loading capacity. Surprisingly, the maximal FITC loading capacity did not correspond to the maximal (positive) ζ-potential shift. In fact, the samples obtained with short conjugation time (ca. 2.5h), corresponding to sub-monolayer lysine conjugation had a disproportionately high dye loading. The maximal FITC loading capacity was achieved at a lysine reaction time of 66h and 19.5h for the 0.5 and 1 ML lysine solutions, respectively (Supporting Materials, Figure S4). This is considerably shorter than the required reaction time to maximize the concentration of surface amino groups (Supporting Materials, S5) and suggest that sub-monolayer surface coverage result in more active (amine) binding sites. Overall, the maximum dye-loading (Supporting Materials, Figure S4 and S6) was achieved with 1 ML lysine concentration and a reaction time of 19.5 h resulting in a dye loading capacity of 2.1 mmol $g^{-1}$, or 1.74 FITC molecules per $nm^2$. This is two orders of magnitude higher than that previously reported for similar non-porous nanostructures. Tat-peptides-iron oxide nanoparticles tagged with FITC, for example, achieved a maximal loading capacity of 0.05 FITC molecules $nm^{-2}$ [47].

Ketoprofen was then loaded onto the amine-terminated nano-agglomerates according to known reactions between ε–$NH_2$ and the ketoprofen –COOH resulting in an amide bond[37] (Figure 4a). A change in zeta potential was observed from unimodal +13mV to a bimodal distribution with peaks at +16mV and -18mV (Figure 4b,c), suggesting loading of ketoprofen.

Journal of Materials Chemistry B Accepted Manuscript

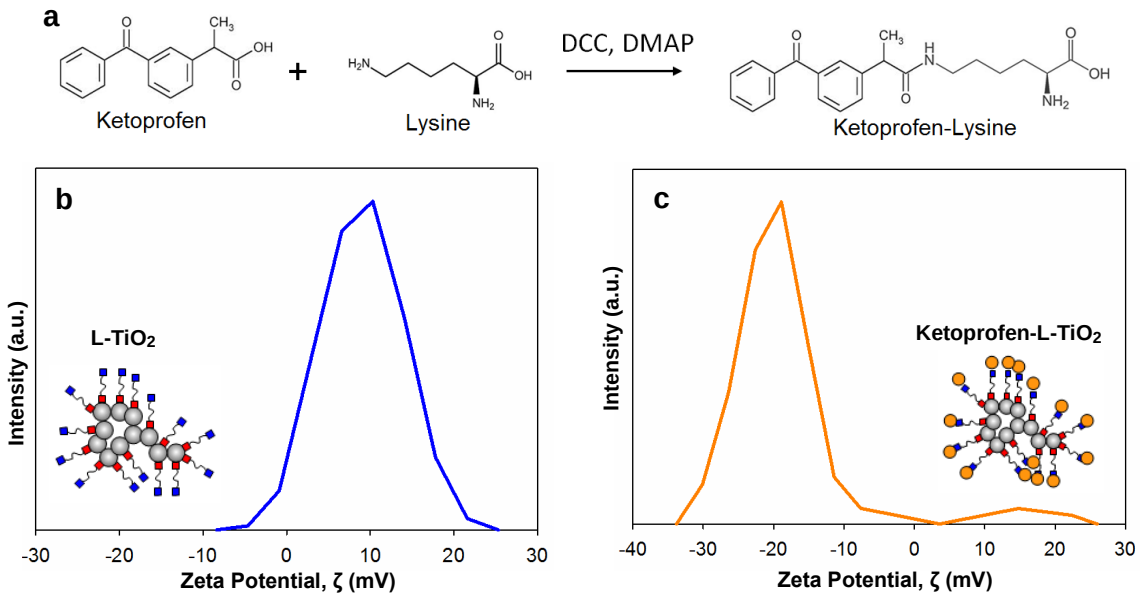


**Figure 4.***(a)Reaction between L-lysine and ketoprofen to form amide bond. Zeta potential distributions of (a) L-$TiO_2$ showing unimodal distribution (+13mV) and (b) Ketoprofren-L-$TiO_2$ showing bimodal distribution (+16mV, -18mV).*

To determine the nanocarrier photo-response, the conjugated samples were exposed to UV light for up to 30s. Elution of lysine into solution was detected over the whole period. This is supported by fluorescamine assays performed on the supernatants (Figure 5a) showing a maximal lysine concentration upon 10s UV exposure. The subsequent fluorescence drop is attributed to the decomposition of the organic molecules in line with the reported photo-catalysys of amino acids by $TiO_2$.[48] Mass spectrometry was performed on supernatants identifying a good match for L-lysine (Figure 5b). The evolution of pipecolinic acid was simultaneously detected, further indicating the partial photo-catalytic conversion of lysine to its cyclization compound[49]. The observed response to increasing UV exposure time indicates the potential for in-vivo time-controlled and targeted drug release by electromagnetic radiation such as by X-ray computed tomography in the timescale $t < 10$ s[20]. Additionally, FTIR was performed on the dried $TiO_2$ powders after UV exposure (Figure 5c). A nearly complete removal of all the organic peaks associated with L-lysine was observed with some potential organic residuals at 2925$cm^{-1}$ and 1645$cm^{-1}$. This was accompanied by changes in the flocculation dynamics and surface charging of the agglomerates after UV exposure. Upon 20s exposure, the DLS agglomerate size distribution (Figure 5d) of the 0.5 ML lysine-$TiO_2$ ($t_r$ = 120h) shifted from trimodal back to unimodal. This distribution was very similar to that of the as-prepared powders. In line with these results, their ζ-potential (Figure 5f) decreased from ca. -12 mV of the acidic conjugated samples back to -35 ± 1 mV, close to that (-40 mV) of the as-prepared $TiO_2$. Analysis of the photo-response dynamics (Figure 5e) indicated an asymptotic decrease in hydrodynamic diameter ($d_H$) within the first 30s of UV exposure with $d_H$ decreasing from 1100 nm of the 0.5 ML (tr = 120h) acidic conjugated samples to ca. 400 nm. This photo-response was consistent for all nanocarriers before and after loading of the FITC (Figure 6a-c) and demonstrates the successful photocleavage of the (ligand) lysine molecules from the $TiO_2$ surface.

Journal of Materials Chemistry B Accepted Manuscript

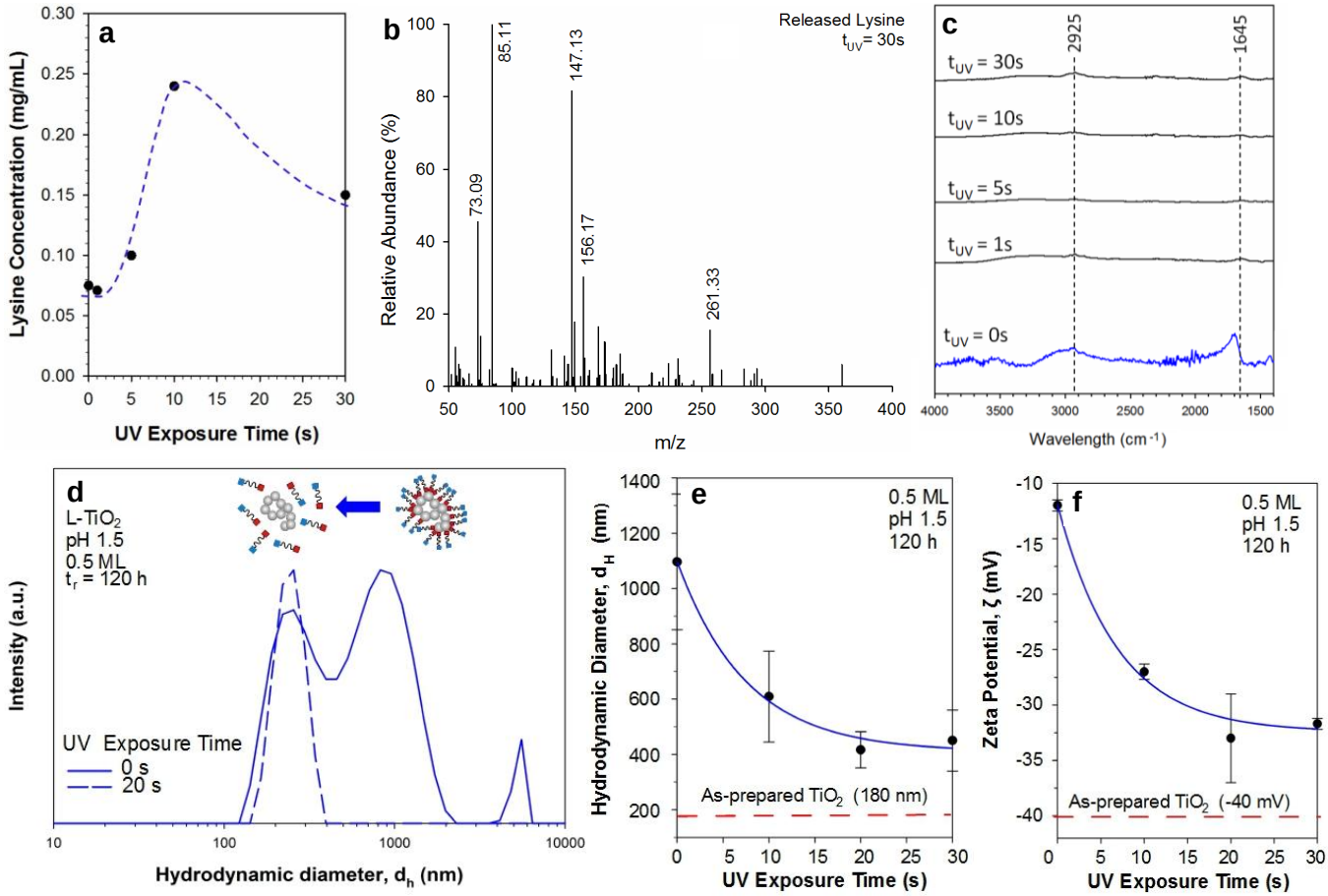


**Figure 5**. Elution of L-lysine in solution upon UV exposure as obtained by (a) fluorescamine fluorescence assay and (b) GC-MS spectra identifying the released L-lysine. FTIR performed on $TiO_2$ powders (c) as a function of UV exposure. Lysine-conjugated $TiO_2$ size distributions (pH 1.5, 0.5 ML, $t_r$ =120h) (d) before and after 20s UV exposure demonstrating photo-induced release of the ligand, and (e) average hydrodynamic diameter and (f) zeta potential of L-$TiO_2$ as a function of UV exposure time.

FITC and ketoprofen loaded L-$TiO_2$ was subject to similar UV exposure conditions. It was found that FITC-L-$TiO_2$ underwent similar de-agglomeration behavior as L-$TiO_2$ (Figure 6a-c), suggesting that the UV-triggered release of adsorbed lysine can then be applied to release of an end-loaded molecule. GC-MS performed on ketoprofen-L-$TiO_2$ liquid phases after UV exposure. At 30 s UV exposure, a main peak appearing after 18 minutes retention time (Figure 6d) matching closely that of ketoprofen standards (m/z = 282) was detected (Figure 6e). Other prominent peaks (notably m/z = 73.11) are attributed to the GC-MS column background, and are also present in the spectrum obtained for released lysine (Figure 5b). This peak was reduced in magnitude by two orders of magnitude in control sample without UV exposure. This suggests the successful elution of ketoprofen into solution that is triggered by UV light.

Journal of Materials Chemistry B Accepted Manuscript

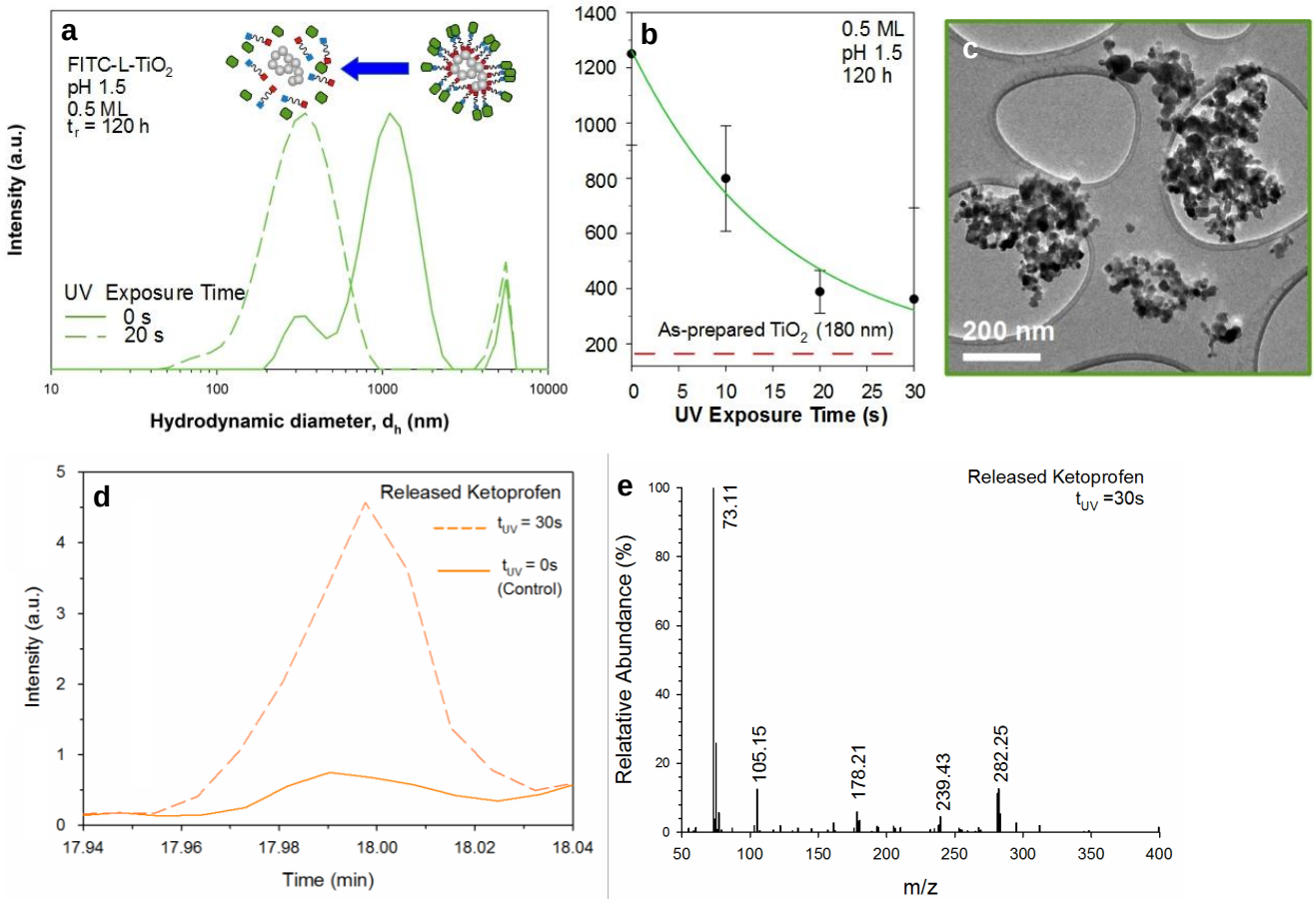


**Figure 6.** FITC loaded L-$TiO_2$ size distributions (a) before and after 20s UV exposure. Average hydrodynamic diameter (b) as a function of UV exposure time and (c) TEM analysis of FITC-loaded L-$TiO_2$ after 20s UV exposure demonstrating the successful release and $TiO_2$ de-agglomeration. Ketoprofen elution after UV exposure of ketoprofen-lysine-$TiO_2$ showing (d) characteristic peak at 18 minutes for control (solid orange line) and 30s UV exposure (broken orange line), and (e) spectra of eluted ketoprofen after 30s exposure.

### 3.3 Intracellular Imaging

To assess the performance of these nanocarrier for intracellular studies, FITC-loaded $TiO_2$ agglomerates were allowed to diffuse into Wistar rat 2/3 pyramidal neurons and imaged with a two-photon microscope[50] (Figure 7c,d). Neurons with alkaline (pH 9) conjugated $TiO_2$ agglomerates showed extremely low fluorescence (Figure 7c). This was attributed to the large agglomerate size (Figure 2c,d) and unreactive surface of the encapsulated samples. In fact, very few nanocomposites were sufficiently small to diffuse through the patch-pipette (Figure 7c) and penetrate the neuron membrane. These suboptimal nanocarriers had poor diffusion into the cell structures, with no visible penetration into the dendritic compartments. Their distribution within the cell was not uniform, showing small regions of higher intensity that, however, had small total fluorescence. As a result, alkaline conjugation and formation of polylysine was found to drastically decrease the nanocarriers performance both with respect to functional molecule loading capacity and intracellular delivery potential.

Journal of Materials Chemistry B Accepted Manuscript

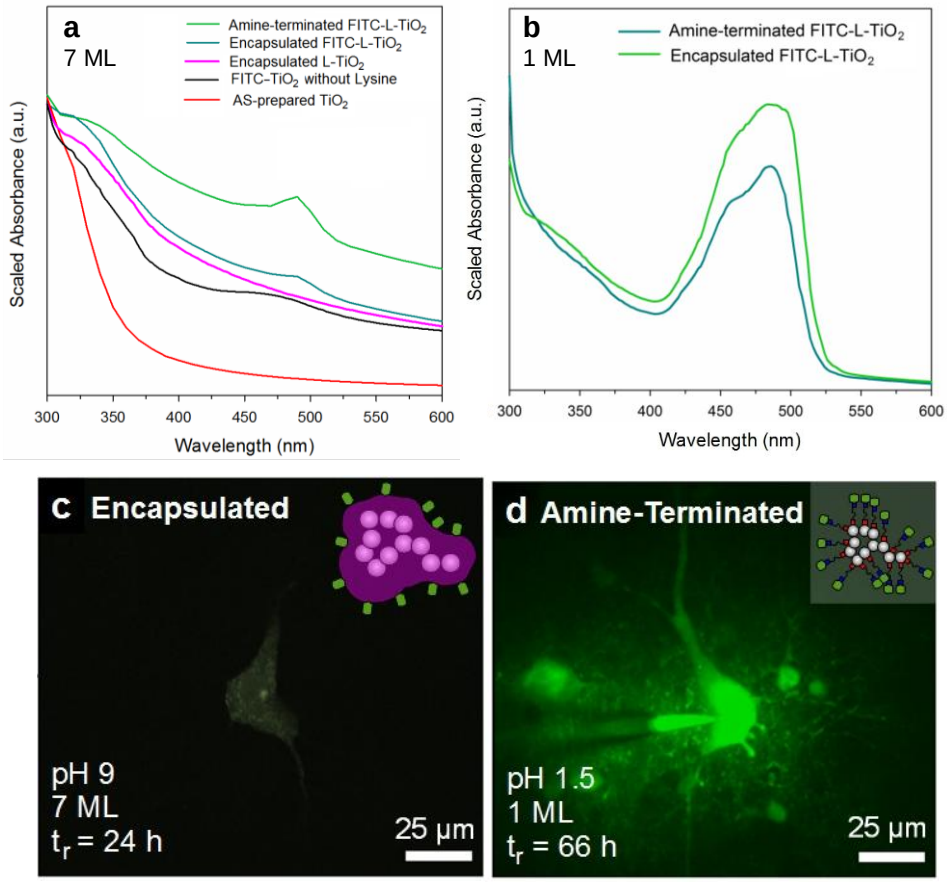


**Figure 7.** Optical absorbance spectra of FITC-loaded nanocarriers with (a) 7 ML lysine concentration and (b) 1 ML lysine concentration for: as-prepared $TiO_2$ (red), FITC-$TiO_2$ without lysine (black) showing minimal direct adsorption of FITC dye, encapsulated $TiO_2$ (magenta), FITC-L-$TiO_2$ in encapsulated morphology (dark green) and FITC-L-$TiO_2$ in amine-terminated morphology (light green). Imaging of pyramidal neurons injected with FITC-L-$TiO_2$ in (c) encapsulated morphology, and (d) amine-terminated morphology.

Conversely, $TiO_2$ agglomerates conjugated in acidic (pH 1.5) conditions (Figure 7d) had a strong fluorescence, comparable in intensity to that of the pure FITC dye solutions (not shown). Upon patching the cell (Figure 7d), they rapidly diffused in the neuron enabling imaging of the dendrites (0.5-5 µm in diameter). Furthermore, the resulting fluorescence was very homogeneous indicating nanocarrier stability and no in-cell flocculation. These results demonstrate for the first time that optimally conjugated flame-made $TiO_2$ agglomerates having low coverage of lysine molecules have potential for highly performing intracellular imaging and photo-induced time-controlled delivery. No immediate toxic effect of the injected FITC-lysine-$TiO_2$ was observed. The cell lifespan was not reduced with respect to previous laser-illumination experiments such as two-photon laser uncaging of neurotransmitters.[50, 51] These results are in line with recent cytotoxicity studies on organic-coated $TiO_2$ agglomerates.[52, 53]

## 4. Conclusions

A versatile photo-responsive nanocarrier platform able to load anti-inflammatory drug ketoprofen and standard imaging dye FITC was synthesized by termination of flame-made $TiO_2$ agglomerates with highly reactive amine surface groups. It was found that low lysine coverage leads to not-encapsulated optimally-sized nanocarriers with high load capacity (up to 2.1 mmol $g^{-1}$) and excellent dispersibility. This was attributed to promotion of carboxylic-binding and inhibition of polylysine formation in acidic conditions (pH 1.5). Efficient photo-induced time-controlled release was demonstrated by complete photo-cleavage of

Journal of Materials Chemistry B Accepted Manuscript

the ligand upon short (≤ 20s) exposure to UV light, eluting lysine and lysine modified ketoprofen. Neurons imaging was achieved by loading of a standard fluorescent dye demonstrating rapid diffusion of the nanocomposites down to the smallest cell dendrites. These results show that these scalable flame-made nanocarriers offer a flexible delivery platform with potential for in-vivo photo-induced time-controlled and targeted release of functional molecules such as required by several anti-cancer drugs and growth factors.

**Acknowledgments**

We would like to acknowledge the Centre of Advanced Microscopy of the Australian National University for electron microscopy imaging and the MEC ANU infrastructure scheme for funding the Nano&Bio Facility at the NRL laboratories. Thanks go to Dr. Charles Hocart of the Research School of Biology, the Australian National University for mass spectrometry.

**References**

1. X. Sun, Z. Liu, K. Welsher, J. T. Robinson, A. Goodwin, S. Zaric and H. Dai, *Nano Res.*, 2008, **1**, 203-212.
2. J. D. Gibson, B. P. Khanal and E. R. Zubarev, *J. Am. Chem. Soc.*, 2007, **129**, 11653-11661.
3. P. Ghosh, G. Han, M. De, C. K. Kim and V. M. Rotello, *Adv. Drug Delivery Rev.*, 2008, **60**, 1307-1315.
4. B. Chertok, B. A. Moffat, A. E. David, F. Yu, C. Bergemann, B. D. Ross and V. C. Yang, *Biomaterials*, 2008, **29**, 487-496.
5. S. Sershen, S. Westcott, N. Halas and J. West, *J. Biomed. Mater. Res.*, 2000, **51**, 293-298.
6. A. K. Patri, I. J. Majoros and J. R. Baker Jr, *Curr. Opin. Chem. Biol.*, 2002, **6**, 466-471.
7. S. V. Vinogradov, T. K. Bronich and A. V. Kabanov, *Adv. Drug Delivery Rev.*, 2002, **54**, 135-147.
8. M. E. Wieder, D. C. Hone, M. J. Cook, M. M. Handsley, J. Gavrilovic and D. A. Russell, *Photochem. Photobiol. Sci.*, 2006, **5**, 727-734.
9. E. R. Gillies and J. M. Fréchet, *Bioconjugate Chem.*, 2005, **16**, 361-368.
10. S. Yang, N. Li, D. Chen, X. Qi, Y. Xu, Y. Xu, Q. Xu, H. Li and J. Lu, *J. Mater. Chem. B*, 2013, **1**, 4628-4636.
11. H. Xu, F. Meng and Z. Zhong, *J. Mater. Chem.*, 2009, **19**, 4183-4190.
12. S. Kapoor and A. J. Bhattacharyya, *J. Phys. Chem. C*, 2009, **113**, 7155-7163.
13. C. Alvarez-Lorenzo, L. Bromberg and A. Concheiro, *Photochem. Photobiol.*, 2009, **85**, 848-860.
14. J. L. Vivero-Escoto, I. I. Slowing, C.-W. Wu and V. S.-Y. Lin, *J. Am. Chem. Soc.*, 2009, **131**, 3462-3463.
15. Y. Yang, B. Velmurugan, X. Liu and B. Xing, *Small*, 2013, **9**, 2937-2944.
16. N. Ž. Knežević, B. G. Trewyn and V. S. Y. Lin, *Chem.--Eur. J.*, 2011, **17**, 3338-3342.
17. N. Z. Knezevic, B. G. Trewyn and V. S. Y. Lin, *Chem. Commun.*, 2011, **47**, 2817-2819.
18. A. Jana, K. S. P. Devi, T. K. Maiti and N. D. P. Singh, *J. Am. Chem. Soc.*, 2012, **134**, 7656-7659.
19. T. Berger, M. Sterrer, O. Diwald, E. Knözinger, D. Panayotov, T. L. Thompson and J. T. Yates, *J. Phys. Chem. B*, 2005, **109**, 6061-6068.
20. F. Schmidt-Stein, R. Hahn, J.-F. Gnichwitz, Y. Y. Song, N. K. Shrestha, A. Hirsch and P. Schmuki, *Electrochem. Commun.*, 2009, **11**, 2077-2080.
21. R. Strobel, A. Baiker and S. Pratsinis, *Adv. Powder Tech.*, 2006, **17**, 457-480.
22. A. Tricoli, A. S. Wallerand and M. Righettoni, *J. Mater. Chem.*, 2012, **22**, 14254-14261.
23. A. Tricoli, M. Righettoni and S. E. Pratsinis, *Langmuir*, 2009, **25**, 12578-12584.
24. CabralH, MatsumotoY, MizunoK, ChenQ, MurakamiM, KimuraM, TeradaY, M. R. Kano, MiyazonoK, UesakaM, NishiyamaN and KataokaK, *Nat. Nano.*, 2011, **6**, 815-823.
25. H. Lee, H. Fonge, B. Hoang, R. M. Reilly and C. Allen, *Mol. Pharm.*, 2010, **7**, 1195-1208.
26. Y. Geng, P. Dalhaimer, S. Cai, R. Tsai, M. Tewari, T. Minko and D. E. Discher, *Nat. Nanotechnol.*, 2007, **2**, 249-255.
27. N. Nakayama and T. Hayashi, *Colloids Surf. A*, 2008, **317**, 543-550.
28. Q. Qu, H. Geng, R. Peng, Q. Cui, X. Gu, F. Li and M. Wang, *Langmuir*, 2010, **26**, 9539-9546.
29. E. Farfan-Arribas and R. J. Madix, *J. Phys. Chem. B*, 2003, **107**, 3225-3233.
30. J. Zhao, M. Milanova, M. M. C. G. Warmoeskerken and V. Dutschk, *Colloids Surf. A*, 2012, **413**, 273-279.
31. G. Guerrero, P. Mutin and A. Vioux, *Chem. Mater.*, 2001, **13**, 4367-4373.
32. G. Minigo, A. Scholzen, C. K. Tang, J. C. Hanley, M. Kalkanidis, G. A. Pietersz, V. Apostolopoulos and M. Plebanski, *Vaccine*, 2007, **25**, 1316-1327.
33. A. Maruyama, T. Ishihara, J.-S. Kim, S. W. Kim and T. Akaike, *Bioconjugate Chem.*, 1997, **8**, 735-742.
34. M. Babic, D. Horák, M. Trchová, P. Jendelová, K. Glogarová, P. Lesný, V. Herynek, M. Hájek and E. Syková, *Bioconjugate Chem.*, 2008, **19**, 740-750.
35. M. Gynther, K. Laine, J. Ropponen, J. Leppänen, A. Mannila, T. Nevalainen, J. Savolainen, T. Järvinen and J. Rautio, *J. Med. Chem.*, 2008, **51**, 932-936.
36. W. Langel and L. Menken, *Surf. Sci.*, 2003, **538**, 1-9.

Journal of Materials Chemistry B Accepted Manuscript

37. M. Gynther, A. Jalkanen, M. Lehtonen, M. Forsberg, K. Laine, J. Ropponen, J. Leppänen, J. Knuuti and J. Rautio, *Int. J. Pharm.*, 2010, **399**, 121-128.
38. A. Tricoli and T. D. Elmøe, *AIChE Journal*, 2012, **58**, 3578-3588.
39. R. Kavitha, S. Meghani and V. Jayaram, *Mater. Sci. Eng. B*, 2007, **139**, 134-140.
40. A. Teleki, S. E. Pratsinis, K. Kalyanasundaram and P. I. Gouma, *Sens. Actuators B*, 2006, **119**, 683-690.
41. H. Keskinen, A. Tricoli, M. Marjamäki, J. M. Mäkelä and S. E. Pratsinis, *J. Appl. Phys.*, 2009, **106**, -.
42. P. Selvakannan, S. Mandal, S. Phadtare, R. Pasricha and M. Sastry, *Langmuir*, 2003, **19**, 3545-3549.
43. V. S. Murthy, J. N. Cha, G. D. Stucky and M. S. Wong, *J. Am. Chem. Soc.*, 2004, **126**, 5292-5299.
44. M. Kar, P. S. Vijayakumar, B. L. V. Prasad and S. S. Gupta, *Langmuir*, 2010, **26**, 5772-5781.
45. M. Rozenberg and G. Shoham, *Biophys. Chem.*, 2007, **125**, 166-171.
46. L. J. Bellamy, *The infrared spectra of complex molecules*, John Wiley and Sons, London, 1957.
47. M. Lewin, N. Carlesso, C.-H. Tung, X.-W. Tang, D. Cory, D. T. Scadden and R. Weissleder, *Nat Biotech*, 2000, **18**, 410-414.
48. H. Hidaka, S. Horikoshi, K. Ajisaka, J. Zhao and N. Serpone, *J. Photochem. Photobiol. A*, 1997, **108**, 197-205.
49. B. Pal, S. Ikeda, H. Kominami, Y. Kera and B. Ohtani, *J. Catal.*, 2003, **217**, 152-159.
50. M. A. Go, C. Stricker, S. Redman, H.-A. Bachor and V. R. Daria, *J. Biophotonics*, 2012, **5**, 745-753.
51. M. A. Go, M.-S. To, C. Stricker, S. Redman, H.-A. Bachor, G. Stuart and V. Daria, *Front. Cell. Neurosci.*, 2013, **7**.
52. M. Hamzeh and G. I. Sunahara, *Toxicol. in Vitro*, 2013, **27**, 864-873.
53. S. Dalai, S. Pakrashi, R. S. S. Kumar, N. Chandrasekaran and A. Mukherjee, *Toxicol. Research*, 2012, **1**, 116-130.


Journal of Materials Chemistry B Accepted Manuscript